DEFORMATION KINEMATICS OF TIBETAN PLATEAU DETERMINED FROM GPS OBSERVATIONS

Jinwei Ren

Institute of Geology, China Seismological Bureau, Beijing 100029 China
Tel: (10)62009095; Fax: (10)62009003; email: jwren@163jb.com

By modeling the complete horizontal strain rate field of the Tibetan plateau with the velocity boundary constraints from plate motions, GPS, and VLBI data, the velocity field of the active deformation in China mainland within a Eurasian reference frame is determined. Robust features in the model are 18-25mm/yr of compression across the Himalayas, 1-4mm/yr of extension across the Baikal rift, 11-14mm/yr of compression across the Tien Shan, and only 7-10mm/yr of left-lateral strike-slip motion on the Altyn Tagh fault zone. The compression across the Himalayas absorbs almost half of the relative motion between India and Eurasia, the Tien Shan takes up about one fourth, and less than one fourth is absorbed across the Altyn Tagh. This means that more than 75% of the north-south shortening between India and Eurasia is absorbed by crustal thickening strains.

Key words: **Crustal deformation GPS Tibet plateau**

1. Introduction

Although it is generally agreed that the north-south shortening induced by the northward penetration of continental India is absorbed by both the thickening of the crust and strike-slip faulting, the relative role and importance of these two processes remains controversial. There is also disagreement on the magnitude of eastward motion of south China and southeast Asia and the role that this eastward displacement plays in accommodating India-Eurasia motion. In this paper, we estimate the complete horizontal velocity gradient tensor field in Tibetan plateau, extending the area of analysis to include all of deforming China mainland as well as the plate boundary zones between Indian and Eurasia plates. Our goal is to determine how the strains are distributed throughout all of the plate boundary zones between India-Eurasia and Arabia-Eurasia and model the plate boundary geometry with irregular grids and separate the different geological units more accurately. In so doing, we hope to obtain a better understanding of the role of various structural zones in accommodating plate motion, address questions related to the magnitude of the motion of Tibetan plateau and southeast China, and speculate on the possible driving mechanism of this motion.

2. Method and Data

Haines and Holt demonstrated how strain rates inferred from seismic moment tensors could be used to retrieve the velocity gradient tensor field[1]. In this study we use Haines' s improved method which uses bicubic Bessel interpolations to match distributions of rates of strain, and which also accommodates potential rapid spatial variations in the strain rate field and allows for irregular grid geometry that better accommodate the shapes of tectonic zones and plate boundaries[2]. The grid geometry is set up to separate different geological areas according to the distribution of earthquake mechanisms and distribution of major Quaternary fault zones (Figures 1). For the regions dominated by major faults or fault zones, such as the plate boundaries, the Altyn Tagh fault, the Tien Shan, and the areas surrounding the Ordos block, the grid areas are constructed to follow the fault zones. The rate of seismicity during this century has been low within the region around the northeastern China and eastern Mongolia, suggesting low deformation rates within the area. We thus approximate this area as rigid and hereafter it is referred to as the northeast China block. The Arabian and Indian plates (the southern extreme of the model), and the Siberia block (the northern extreme of the model) are also constrained to be rigid.

Figure 1

Earthquake moment tensors (Figure 1) are the most reliable observation that constrain the style of crustal deformation within the upper deforming brittle layer (top 20 km). Earthquakes generally indicate the directions of principal strains, they indicate whether crustal thickening or thinning are present, and they show where the deformation is strike-slip, compression, or extension. Quaternary faults can also provide important information on the style of the strain rate tensor. We use both earthquake moment tensors and Quaternary fault slip rates to place constraints on the expected style of the strain rate tensor within all areas in deforming China mainland. In addition, we also incorporate Global Positioning System (GPS) observations into some of our analyses.

Haines have outlined a method of using *a priori* information for calculating the variance-covariance matrix in order to constrain the deformation style and magnitude[2]. There are three levels of constraints. The first level amounts to having no constraints on the style of deformation in which case the same level of variance is given to the three strain rate components (isotropic). The second case amounts to constraining the orientation of the principal axes of the horizontal strain rate tensor. The third case amounts to constraining the relative magnitudes of the two principal axes, which is equivalent to constraining the style of the earthquake mechanisms or the style of deformation. The second and third cases amount to successively more anisotropic behavior of the straining medium.

Mechanisms for earthquakes from 1976 to 2000 are from the Harvard Centroid Moment Tensor (CMT) catalogue[3]. For events that occurred primarily between 1964 and 1976 moment tensor estimates are obtained from a number of studies which is documented by Holt *et al*.[4]. Historical earthquake data within China have been well summarized by Molnar and Deng[5]. The geodetic data that are incorporated as observations to be fitted by our model include the GPS measurements in the China from the Crustal Movement Observation Network of China (CMONC), Tien Shan[6], and northern China[7]. The 25 fiducial GPS stations of CMONC began to operate since 1998. The 56 basic GPS stations were occupied twice in 1998 and 2000 respectively. The reference frame for all the GPS and VLBI data is the stable Eurasian plate.

3. Solution 1: NUVEL-1A Constraints Alone

We first perform a constrained inversion in which the India and Arabian plates rotate relative to the Eurasian plate about their respective Euler poles defined by the NUVEL-1A model[8]. The strain rate field for this solution is shown in Figure 2a. In this isotropic case, the strain rate field is dominated by roughly north-northeast compressional strain rates in China mainland and the surrounding areas, which is the direct response of India plate plate motion. Although the general pattern of the strain rate field is acceptable, this solution fails to match the observations in several aspects. First, there is no E-W extension within southern Tibet. Second, strike-slip strains given by the fitted strain rate field within the areas containing the Altyn Tagh, east Kunlun, Xianshuihe and Saging faults are not prominent (Table 1). Third, strain rates around the Ordos block involve north-northeast compression rather than the extensional deformation observed there, and extensional strain rates are also absent in Baikal.

Figure 2a, b

Figure 2b shows the velocity field relative to Siberia associated with the strain rates in Figure 2a. The southeast China moves slowly east-northeast at a rate of about 4mm/yr. The predicted velocity at Shanghai is 3.7mm/yr in a direction of 74°, whereas the and Very Long Baseline Interferometry (VLBI) velocity there is 8 - 11mm/yr in a direction of 110~123° [9]. There is almost no south-southeast extension in the Baikal region.

In order to investigate how much of the north-south shortening between India and Asia is accommodated by the strike-slip motion, we calculate the total rate of north-south contraction accommodated by strike-slip strains along several profiles in longitude. The ratios of strike-slip strains to the total traction associated with all strains, along longitudes 78°E, 83°E, 90°E and 96°E are shown in Table 2. In this solution 1, strike-slip related strains accommodate on average about 12% of the north-south shortening. The solution 1 shows the NUVEL-1A motion of India relative to Eurasia is being absorbed almost entirely by crustal thickening strains.

4. Solution 2: Adding Constraints from Earthquake Mechanisms and Incorporating Geodetic Observations

An inversion, with the same plate velocity boundary conditions as in the last solution, along with the GPS measurements in China (from CMONC), Tien Shan, northern China, and the VLBI measurements at Shanghai, is performed such that the region will strain in the direction and style dictated by the distribution of earthquake mechanisms. The inclusion of geodetic data, as well as the constraints on the style of the strain rate, provides a solution that is in closer accord with the observed deformation field in several aspects (Figure 3a). The match with the deformation field is not as completely trivial as it may seem since the sense of motion on faults that would correspond to the fitted strain rate field is not prescribed *a priori*. That is, only the relative sizes and directions of the two principal strain rate axes in each grid area are prescribed, not the sign of principal strain rates.

Figure 3a, b

In this solution the Tibetan Plateau now has a component of strain rate that involves E-W extension (Figure 3a). These rates accommodate a total of 13mm/yr of extension across the entire southern Tibetan Plateau between the longitudes of about 78°E and 95°E. The predicted strain rates in East Tibet correspond to rates of left-lateral strike-slip faulting that are now in accord with observation on the east Kunlun and Xianshuihe faults (Table 1b). The compressional velocity across the Himalayas is about 18mm/yr at the western segment, 21mm/yr in the middle, and 25mm/yr at eastern segment (Table 1b). These rates are almost half of the India plate motion velocity relative to Siberia and are in agreement with GPS rates of motion observed across the Himalayas. The fitted velocity field gives rates of total shortening in the Tien Shan of about 11-14mm/yr, less than the estimate of ~20mm/yr based on the fitted GPS measurements[6]. Although the Altyn Tagh fault has left-lateral strike-slip motion, the predicted slip rate of 6-9mm/yr is almost three times lower than has been inferred, but fits the GPS observation quite well. This solution gives extension rates of about 4mm/yr across Baikal which is in accord with the GPS observations, as well as extension in the regions surrounding the Ordos block.

In this solution, the southeast China block rotates anticlockwise about a pole of rotation at (65°N, 132°E, 0.1deg/Myr), which gives an eastward motion to the south China relative to Siberia of about 8mm/yr (Figure 3b). The northeast China block rotates anticlockwise about a pole at (60°N, 125°E, 0.12 deg/Myr), which gives a slow motion of northeast China at a rate of about 2.8mm/yr in a direction of 106° relative to Siberia and hence southeastward extension of about 4mm/yr across the Baikal rift.

Table 1a Rates of extensional and compressional motion across tectonic regions in China and its surroundings (mm/yr)

	solution 1	solution 2	observation	references
West Himalayas	-16.0	-18.0	-20.5±2	Bilham *et al.*, 1997; Molnar, 1990
Middle Himalayas	-20.0	-20.0	-18±7	
East Himalayas	-23.0	-25.0	-18±7	Molnar, 1990
South Tibet*	0.0	13.0	10	Armijo *et al.*, 1989; Molnar *et al*, 1989
Nan Shan	-7.0	-12.0	-15±6	Meyer *et al.*, 1991
Longmen Shan	-1.0	-2.0	< -5	King *et al.*, 1997
Yinchuan	-0.2	0.8	3.6	Research group on Ordos massif, 1988
Daqing Shan	-0.6	3.0	6	Research group on Ordos massif, 1988
Shanxi	-0.1	0.5	0.8	Deng *et al.*, 1994
Weihe	-0.5	1.5	1.5	Shen-tu *et al.*, 1991
Baikal Rift	0.5	3.0	2~3	England and Molnar, 1997
Altyn Tagh	-10.0	-9.0	-6±4	Molnar *et al.*, 1987
West Tien Shan	-13.0	-14.0	-20±6	Abdrakhmatov *et al.*, 1996
East Tien Shan	-10.0	-11.0	-6±3	Avouac, *et al.*, 1993
Haiyuan	-5.0	-8.0		

* Total E-W extension rate

Table 1b Rates of strike slip motion of major Quaternary faults in China and its surroundings (mm/yr)

	solution 1	solution 2	observation	references
Sagaing	-30.0	-39.0	-42	Bellier *et al.*, 1995
			6.8	Research group on Ordos massif, 1988
Haiyuan	1.0	4.0	5-10	Burchfiel *et al.*, 1991
			8±2	Zhang *et al.*, 1988
Xiaojiang & Zemuhe	1.0	6.0	4~7	Chen *et al.*, 1988; Ren, 1994
Xianshuihe	4.0	9.0	15±5	Allen *et al.*, 1991
East Kunlun	0.5	10.0	10~13	Kidd *et al.*, 1988; Ren *et al.*, 1994
Chaman	18.0	16.0	19~24	Lawrence *et al.*, 1992
			29.8±10	Avouac *et al.*, 1993
West Altyn Tagh	8.0	10.0	20-30	Peltzer *et al.*, 1989
			25	Research group of Altyn Tagh fault, 1992
			29.8±10	Avouac *et al.*, 1993
Central Altyn Tagh	6.0	7.0	16~22	Research group of Altyn Tagh fault, 1992
			9±3	Shen *et al.*, 2001
East Altyn Tagh	4.0	4.0	4±2	Meyer *et al.*, 1996
			12±2	Research group of Altyn Tagh fault, 1992
Red River	-0.5~-2	-1~-4	-2~-4	Allen *et al.*, 1984; Xiang *et al.*, 1994

In the extensional and compressional slip cases, the negative velocities indicate compressional and positive velocities indicate extensional. In the strike slip cases, the negative velocities indicate right lateral and positive velocities indicate left lateral.

In solution 2, the strike-slip motion takes up a maximum of 24% of the north-south shortening along the 96°E profile and 19% on average (Table 2). Accommodating plate motion while taking into account the directions and relative magnitudes of the principal strain rates yields a solution with slight rates of positive dilatation (crustal thinning) in parts of Tibet, and within the Lake Baikal region.

Table 2 The ratio of strike-slip rate to total compressional rate in south-north direction

location (°E)	V_{ss} / V_{tt}	
	Solution1	Solution 2
78	0.12	0.15
83	0.13	0.15
90	0.15	0.26
96	0.09	0.25
average	0.12	0.20

V_{tt} - total compressional rate in south-north direction;
V_{ss} - component of strike slip rate out of V_{tt}.

Figure 4 shows the fit of our model velocities to the GPS observations. Most of the GPS observations are fit within 2-sigma uncertainties. The model velocity vector at Shanghai in this solution is about 8mm/yr in the direction of 97°. This almost fits the VLBI observation at Shanghai.

Figure 4a, b, c

The predicted rates of strike-slip related strain along the Altyn Tagh fault are too low compare with the geological data. Because the style of strain both north and south of Ordos is primarily extensional, and because rates are less than 5mm/yr (see Table 1a), there is a limit to the amount of eastward transfer of motion from the Altyn Tagh into south China. Thus motion on the Altyn Tagh fault must terminate in compression. Moreover, since our predicted rates of compression across the Nan Shan (12mm/yr) in solution 2 are in accord with observation (15 ± 6mm/yr[10]), we suggest that the fitted rates of strike-slip motion along the Altyn Tagh fault of 6 - 9mm/yr are realistic.

5. Discussion and Conclusions

With the increase in rate of anticlockwise rotation of southeast China, which is almost zero in solution 1, there is an increase in the magnitude of strike-slip faulting. This implies that the deformational features in eastern Asia continent, such as strike-slip motion on the Altyn Tagh, East Kunlun, and Xianshuihe faults, as well as extension around the Ordos block and in Baikal, appear to be more a consequence of the anticlockwise rotation of southeast China block relative to Siberia than that of the collision between India and Asia.

In all the anisotropic models, we obtain about 25mm/yr of compression across eastern Himalayas and about 20mm/yr of compression across the western Himalayas. This means that the Himalayas absorb almost half of the relative motion between India and Eurasia. This is not surprising and can be understood by considering that if too little convergence were to occur at the Himalayas, then more deformation would be required within the interior of eastern Asia in order to accommodate plate motion. The additional deformation required within the interior of eastern Asia produces a degraded fit to the expected style and distribution of the rates of strain. Likewise, too much shortening at the Himalayas (in excess of 25 - 30mm/yr) will also produce a degraded fit to the expected distribution of the strain rate tensor field within the interior of eastern Asia.

In our model, the Nan Shan takes up about 12mm/yr of convergence between India and Eurasia (Table 1). Mongolia, north of the Nan Shan, does not absorb any significant component of convergence. Therefore, east Tibet takes up about 16mm/yr of the remaining total convergence rate between east India and Siberia. This result is similar to that obtained from the modeling of Quaternary fault strain rates[10]. Since the Tien Shan takes up 11 - 14mm/yr of convergence, and since the NUVEL-1A convergence rate between India and Eurasia is about 45mm/yr in west central India, only about 10mm/yr of convergence remains for the Altyn Tagh and west Tibet. This is one reason why the calculated left-lateral strike-slip rate along Altyn Tagh is no more than 10mm/yr in all our models (Table 1b).

The source of the rotation of southeast China may not be entirely due to dynamics associated with the collision and the crustal thickness contrasts around Tibet. Although our argument must still be based principally on kinematics, the source for the velocity boundary condition of southeast China appears to be forces other than those associated with the collision, such as forces associated with the subduction process along the eastern margin of southeast Asia, for example, trench rollback between the Philippine Sea Plate and southeast Asia or shear tractions along the base of southeast Asia.

Acknowledgment The author would like to thank Zhu Wenyao for providing GPS observations from CMONC. He is also grateful to B. Holt, B. Shen-Tu and J. Haines for guidance about using the codes. Maps were prepared using GMT version 3.4 by Wessel and Smith. This research was funded by National Key Basic Research Program (G1998040703).

References

[1] Haines, *et al*., A procedure to obtain the complete horizontal motion within zones of distributed deformation from the inversion of strain rate data, *J. geophys. Res.*, 1993: **98**, 12,057-12,082.

[2] Haines, *et al*., Representing distributed deformation by continuous velocity fields, *Sci. Rept. 98/5*, Inst. of Geol. and Nucl. Sci., Wellington, New Zealand, 1998.

[3] Dziewonski, *et al.*, Determination of earthquake source parameters for studies of global and regional seismicity, *J. geophys. Res.*, 1981: **86**, 2825-2852.

[4] Holt, *et al*., Earthquake strain rates and instantaneous relative motions within central and eastern Asia, *Geophys. J. Int*., 1995: **122**, 569-593.

[5] Molnor, *et al*., Faulting associated with large earthquakes and the average rate of deformation in central and eastern Asia, *J. geophys. Res.*, 1984: **93**, 6203-6227.

[6] Abdrakhmatov, *et al*., Relatively recent construction of the Tien Shan inferred from GPS measurements of present-day crustal deformation rates, *Nature*, 1996: **384**, 450-453.

[7] Shen, *et al*., Contemporary crustal deformation in east Asia constrained by Global Positioning System measurements, *J. geophys. Res.*, 2000: **105**, 5721-5734.

[8] DeMets, *et al*., Effect of recent revision to the geomagnetic reversal time scale on estimates of current plate motion, *Geophys. Res. Lett.*, 1994: **21**, 2191-2194.

[9] Heki, Horizontal and vertical crustal movements from three-dimensional very long baseline interferometry kinematic reference frame: Implication for the reversal timescale revision, *J. geophys. Res.*, 1996: **101**, 3187-3198.

[10] Meyer, *et al*., Rate of left-lateral movement along the easternmost segment of the Altyn Tagh fault, east of 96°E(China), *Geophys. J. Int*., 1996: **124**, 29-44.

Figure 1 Earthquakes focal mechanisms and major Quaternary faults in China mainland and its surroundings. The orientation of principal strain axes and the style of strain rates obtained from the earthquake data are used to constrain the deformation style of the area. The slip rate of Quaternary fault is used to quantify the average slip rate in each grid area.

Figure 2(a) Strain rate solution for the case in which no constraints are placed on style and direction of strain in accommodating the plate motions of India-Eurasia and Arabia-Eurasia defined by NUVEL-1A Euler vectors with respect to Eurasia. This solution is analogous to the response of an isotropic Newtonian thin viscous sheet. The magnitude of strain rates are roughly constrained by the variances obtained from the expected model velocities.

Figure 2(b) Velocity field solution relative to Eurasia associated with strain-rate solution in (a). Error ellipses are for one standard error. An anticlockwise rotation relative to Eurasia about a pole of rotation at (58°N, 28°W, 0.04deg/Myr) and north-east motion of southeastern China can be seen.

Figure 3(a) Strain rate field solution that accommodates the defined plate motions and the GPS, VLBI observations in China mainland. The strains are constrained to occur in the style and direction that are consistent with earthquake mechanisms, and hence the solutions are analogous to the response of a generally anisotropic Newtonian thin viscous sheet. This anisotropic model requires that half of the deformation caused by India plate collision be taken up across the Himalayas.

Figure 3(b) Velocity field solution relative to Eurasia associated with strain-rate solution in (a). Error ellipses are for one standard error. An anticlockwise rotation relative to Eurasia about a pole of rotation at (66°N, 132°E, 0.14 deg/Myr) and south-east motion of southeast China can be seen. Once the deformation style obtained from earthquake data is included, the model requires 18-25mm/yr of compression across the Himalayas and less than 10mm/yr of left lateral strike-slip motion along the Altyn Tagh fault zone.

Figure 4 The fit of model velocities to the GPS observations in China (a), northern China(b) and Tien Shan (c). The reference point for the GPS observations are stable Eurasia. The error ellipses are two standard error for both observations and the predicted velocity vectors.

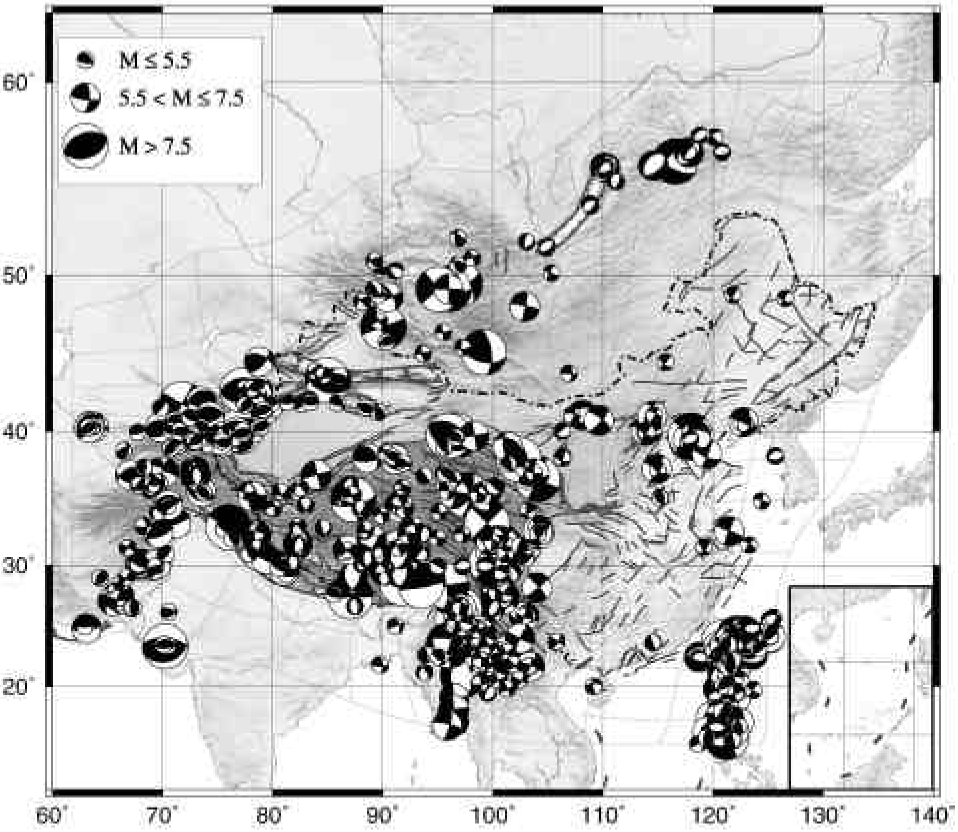

Figure 1

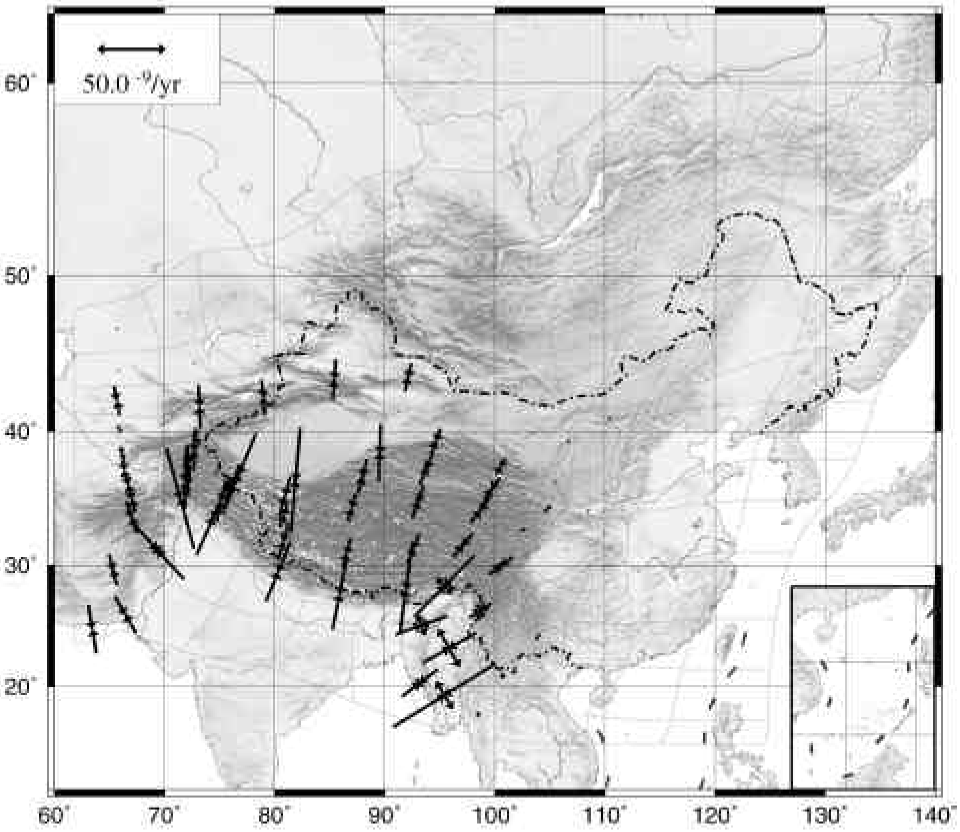

Figure 2a

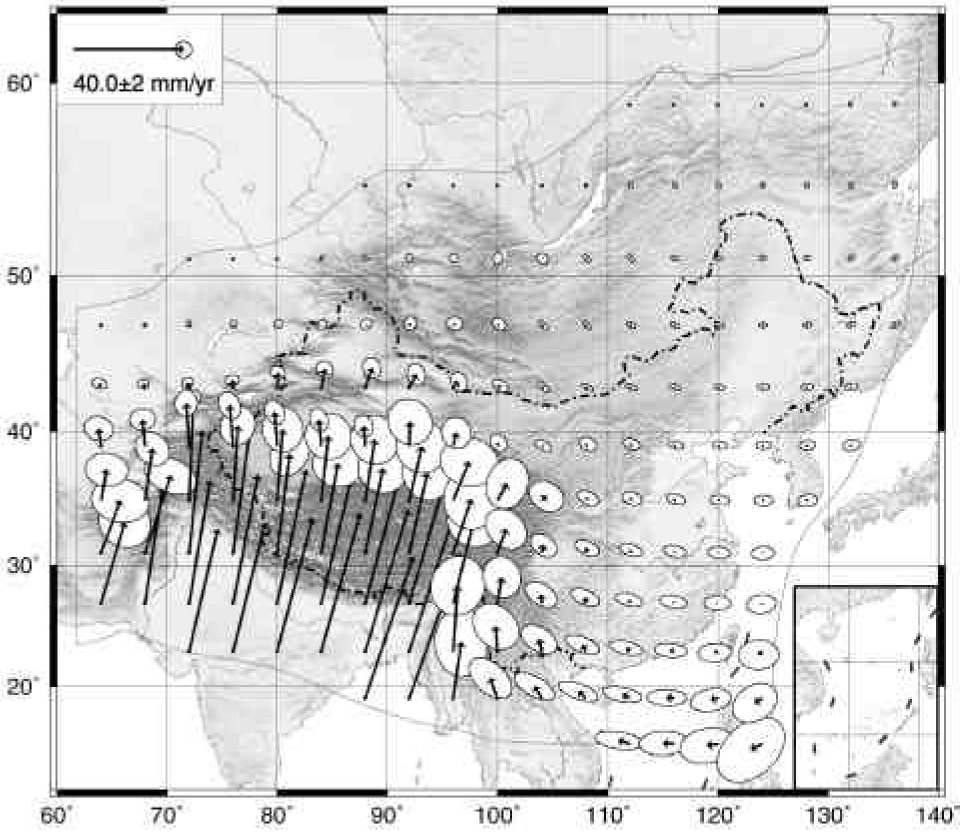

Figure 2b

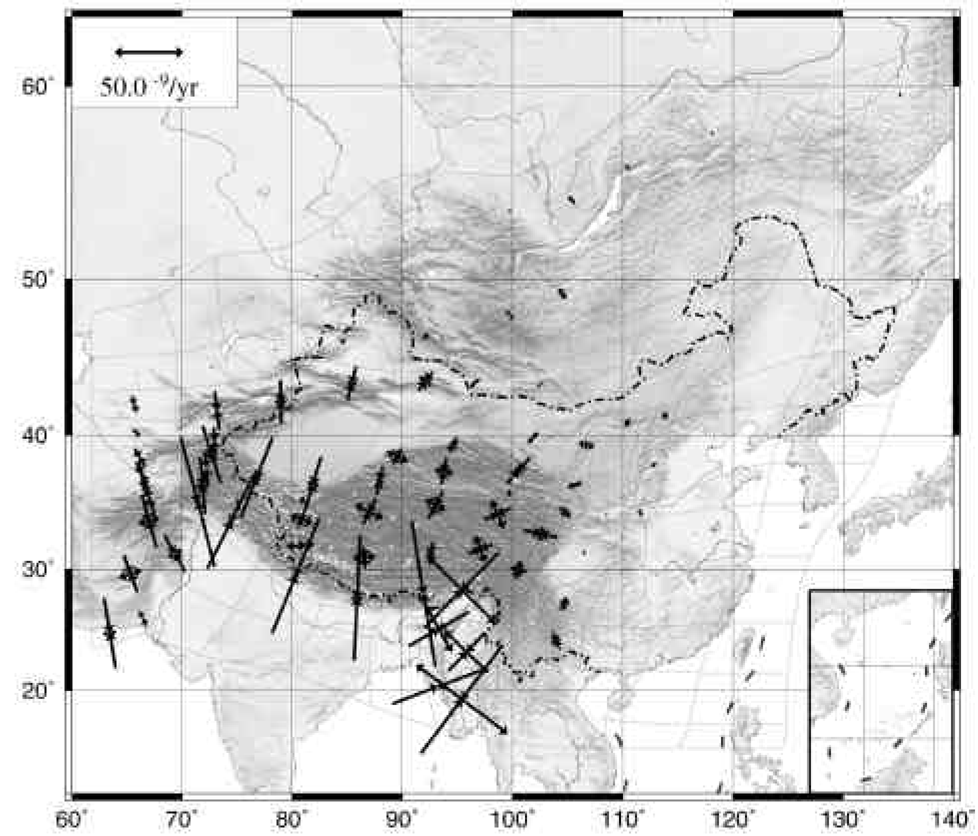

Figure 3a

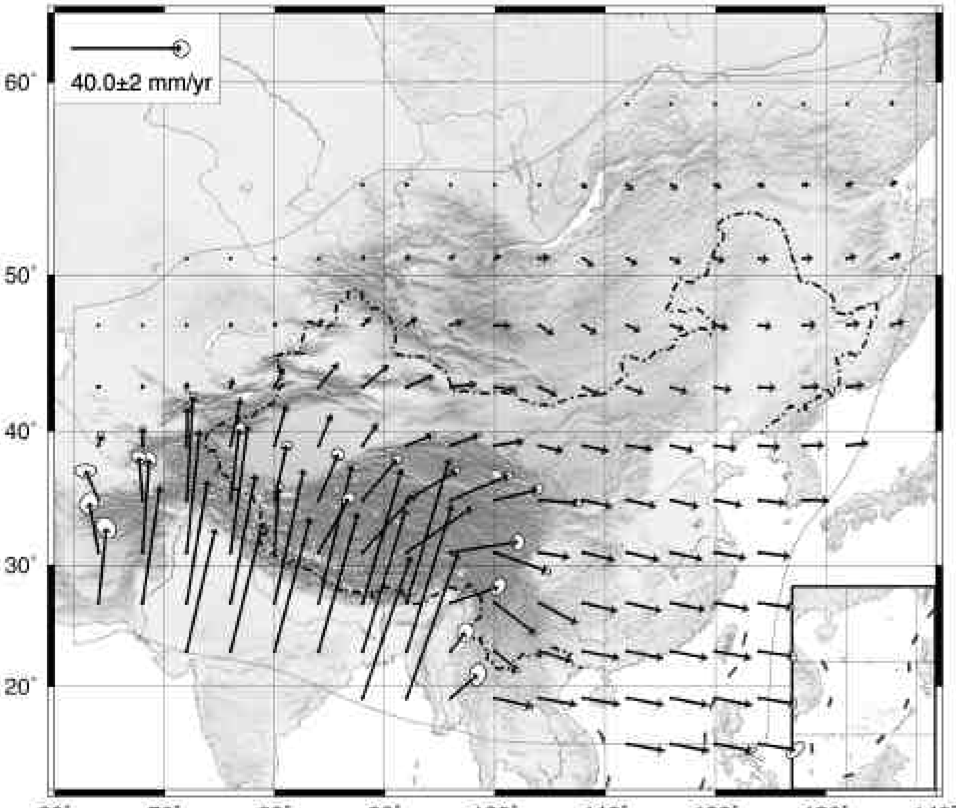

Figure 3b

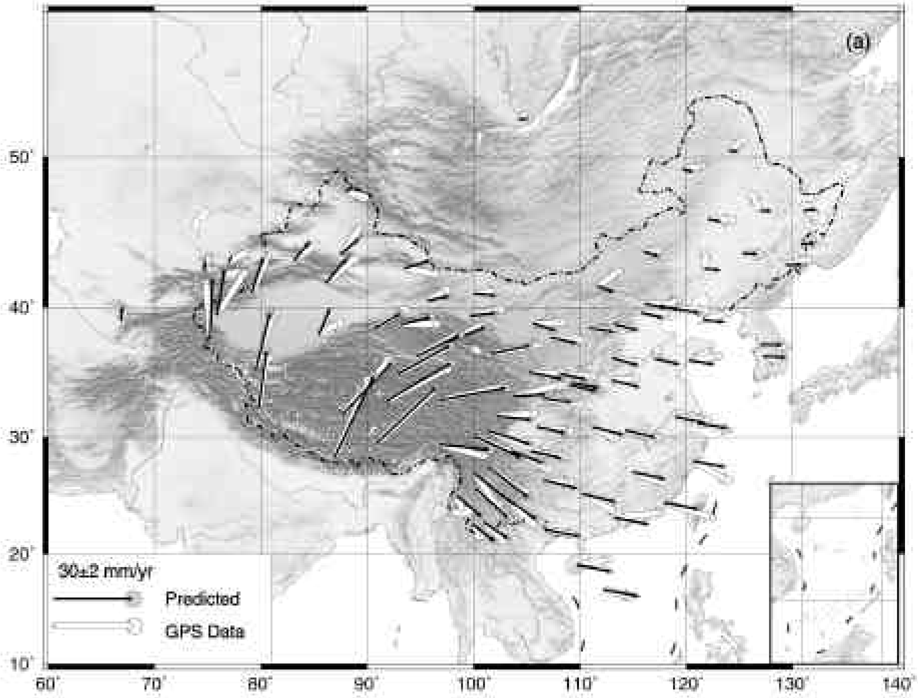

Figure 4a

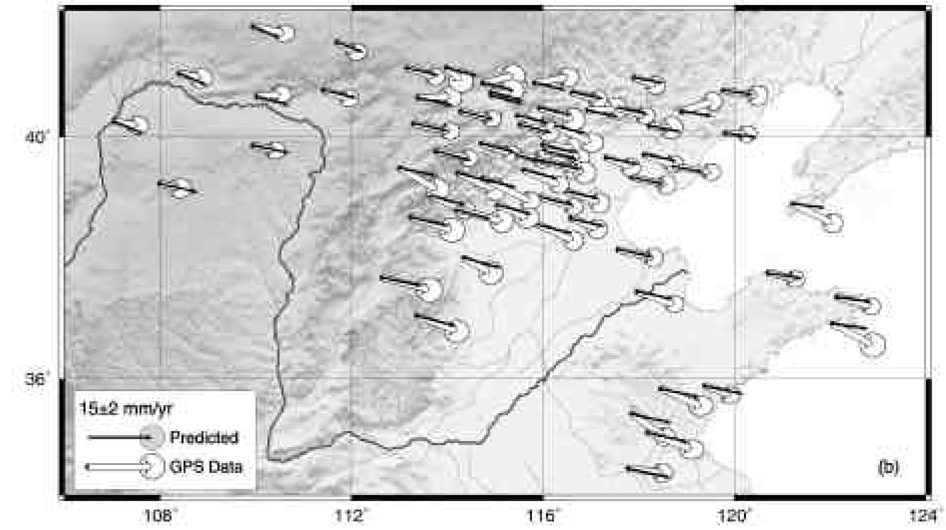

Figure 4b

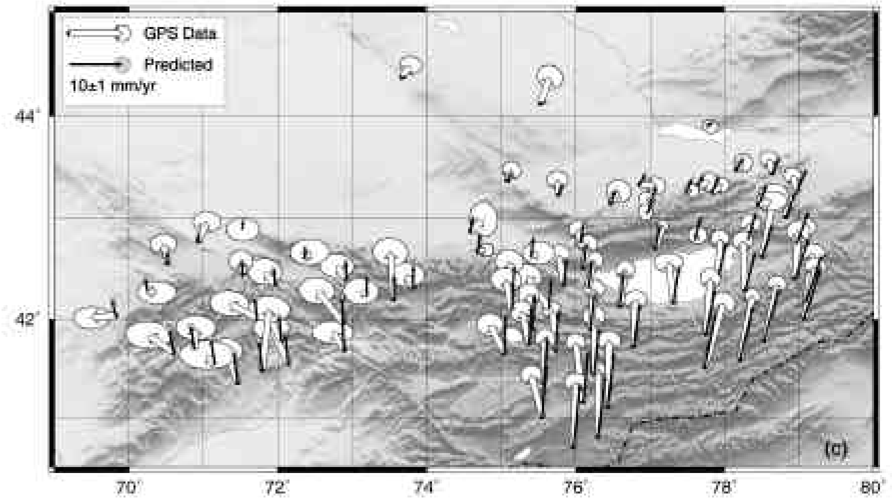

Figure 4c